Atmospheric
Measurement
Techniques
Open Access

EGU

Discussions

Satellite measurements of peroxyacetyl nitrate from the Cross-Track Infrared Sounder: Comparison with ATom aircraft measurements

Vivienne H. Payne[1], Susan S. Kulawik[2], Emily V. Fischer[3], Jared F. Brewer[3,4], L. Gregory Huey[5], Kazuyuki Miyazaki[1], John R. Worden[1], Kevin. W. Bowman[1], Eric J. Hintsa[6,7], Fred Moore[6,7], James W. Elkins[7] and Julieta Juncosa Calahorrano[3]

[1]Jet Propulsion Laboratory, California Institute of Technology, Pasadena, California, USA
[2]Bay Area Environmental Research Institute / NASA Ames, Mountain View, California, USA
[3]Colorado State University, Fort Collins, Colorado, USA
[4]Harvard University, Cambridge, Massachusetts, USA
[5]Georgia Tech, Georgia, USA
[6] Cooperative Institute for Research in Environmental Sciences, University of Colorado Boulder, Boulder, Colorado, USA
[7] Global Monitoring Laboratory, NOAA, Boulder, Colorado, USA

Correspondence to: Vivienne H. Payne (vivienne.h.payne@jpl.nasa.gov)

Abstract. We present an overview of an optimal estimation algorithm to retrieve peroxyacetyl nitrate (PAN) from single field of view Level 1B radiances measured by the Cross-Track Infrared Sounder (CrIS). CrIS PAN retrievals show peak sensitivity in the mid-troposphere, with degrees of freedom for signal less than or equal to 1.0. We show comparisons with two sets of aircraft measurements from the Atmospheric Tomography Mission (ATom), the PAN and Trace Hydrohalocarbon ExpeRiment (PANTHER) and the Georgia Tech Chemical Ionization Mass Spectrometer (GT-CIMS). We find a systematic difference between the two aircraft datasets, with vertically averaged mid-tropospheric values from the GT-CIMS around 14 % lower than equivalent values from the PANTHER. However, the two sets of aircraft measurements are strongly correlated (R^2 value of 0.92) and do provide a consistent view of the large-scale variation of PAN. We demonstrate that the retrievals of PAN from CrIS show skill in measurement of these large-scale PAN distributions in the remote mid-troposphere compared to the retrieval prior. The standard deviation of individual CrIS-aircraft differences is 0.08 ppbv, which we take as an estimate of the uncertainty of the CrIS mid-tropospheric PAN for a single satellite field of view. The standard deviation of the CrIS-aircraft comparisons for averaged CrIS retrievals (median of 20 satellite co-incidences with each aircraft profile) is lower, at 0.05 ppbv. This would suggest that the retrieval error reduces with averaging, although not with the square root of the number of observations. We find a negative bias of order 0.1 ppbv in the CrIS PAN results with respect to the aircraft measurements. This bias does not appear to show a dependence on latitude or season.

1 Introduction

Peroxyacetyl nitrate (PAN) is formed through the oxidation of volatile organic compounds (VOCs) in the presence of nitrogen oxide radicals (NO_x) (Roberts, 2007). PAN formation and decomposition provide important pathways by which NO_x emissions

are redistributed (Singh and Hanst, 1981; Singh et al., 1986) and contribute to downwind oxidant formation (Wang et al., 1998). PAN is a particularly difficult compound to capture and validate in models because many factors impact the production

35 and lifetime of this species (Fischer et al., 2014). PAN has a low background abundance, is often a clear tracer of photochemistry, and its abundance can be highly variable in space and time. Therefore, it can be difficult to know whether the limited in-situ measurements are broadly representative. Aside from a few exceptions (e.g., Fiore et al., 2018; Pollack et al., 2013) PAN is not routinely measured in surface air quality networks. It is often only measured *in situ* as part of relatively short (i.e., weeks to months) field campaigns (e.g., Alvarado et al., 2010; Fischer et al., 2010; Juncosa Calahoranno et al., 2020),

40 aimed at elucidating specific chemical process. Thus existing *in situ* observations provide snapshots of this species, they cannot be used to probe changes over time, and they offer a limited view of the spatial distribution.

Recent work on ground-based remote sensing of PAN from stations of the Network for the Detection of Atmospheric Composition Change (NDACC) provides the promise of long-term measurements, albeit with limited spatial coverage

45 (Mahieu et al., 2021). Satellite remote sensing provides a means for observations over long timescales with global coverage. While limb-sounding satellite observations can provide global-scale information on PAN in the upper troposphere and lower stratosphere with high vertical resolution and sensitivity (Glatthor et al., 2007; Moore and Remedios, 2010; Wiegele et al., 2012; Tereszchuk et al., 2013; Pope et al., 2016; Ungermann et al., 2016), nadir-viewing satellite observations can offer sensitivity to PAN variations lower in the troposphere. Observations and retrievals of PAN have previously been reported

50 from the Tropospheric Emission Spectrometer (TES) (Alvarado et al., 2011; Payne et al., 2014) and from the Infrared Atmospheric Sounding Interferometer (IASI) (Clarisse et al., 2011; Franco et al., 2018). Nadir-viewing observations have shown large enhancements in PAN associated with fires and have been used to shed new light on the role of fires, PAN precursor emissions and dynamics on the global distribution of PAN and on long-range transport of ozone (Zhu et al., 2015, 2017; Payne et al., 2017; Jiang et al., 2016; Fischer et al., 2018).

55

Here we show new retrievals of PAN from the Cross-Track Infrared Sounder (CrIS). We demonstrate the capability of CrIS to measure variations in background PAN levels over the remote ocean. Section 2 provides an overview of the satellite and aircraft measurements used in this work, while Section 3 describes the CrIS PAN retrieval algorithm. Results are presented in Section 4. Section 5 provides discussion of the results and conclusions.

60 ## 2 Measurements

2.1 CrIS satellite radiances

The Cross-Track Infrared Sounder (CrIS) (Han et al., 2013) is a high spectral resolution spectroradiometer. CrIS instruments are currently flying on the Suomi National Polar-Orbiting Partnership (S-NPP) satellite and on the National Oceanic and Atmospheric Administration NOAA-20 satellite as part of the Joint Polar Satellite System (JPSS). CrIS instruments will be

Atmospheric
Measurement
Techniques
Discussions

65   also included on the payload for 3 more JPSS satellites, with a plan to extend the CrIS record to 2035 and beyond. CrIS is a
Fourier transform spectrometer and provides measurements of Earth view interferograms at 30 cross-track positions, each with
a 3 x 3 array of field of views (FOVs). The diameter of the FOVs is 15 km at nadir. The interferograms are processed to provide
calibrated and geolocated Level 1B spectra in three bands: 660-1095 cm^{-1} (longwave), 1210-1750 cm^{-1} (mid-wave) and 2155-
2550 cm^{-1} (shortwave). The full spectral resolution radiances are supplied on a 0.625 cm^{-1} spectral grid.

70

In this work, we use radiances from S-NPP CrIS, although the algorithm described here can be applied to data from any of the
CrIS instruments. We use NASA version 2 Level 1B radiances (Revercomb and Strow, 2018) from the Goddard Earth Sciences
Data and Information Services Center (GES DISC). S-NPP flies in a sun-synchronous orbit with a mean local daytime overpass
time of 13:30. Radiometric calibration is described in Tobin et al. (2013) while the noise characteristics are described in
75   Zavyalov et al. (2013). The CrIS noise is low compared to other high resolution thermal infrared sounders, such as the TES,
IASI, and the Atmospheric Infrared Sounder (AIRS). This low noise, combined with the afternoon orbit, enables good
sensitivity to a range of trace gases (e.g. Shephard and Cady-Pereira., 2015; Fu et al., 2019).

2.2 ATom aircraft measurements

The Atmospheric Tomography Mission (ATom) was a series of aircraft campaigns to study the impact of human-produced air
80   pollution on greenhouse gases and chemically reactive gases in the atmosphere (Wofsy et al., 2018). The mission consisted of
four campaigns, covering four seasons: ATom-1 (July-August 2016), ATom-2 (January-February 2017), ATom-3 (September-
October 2017) and ATom-4 (April-May 2018). An extensive payload was deployed on the NASA DC-8 aircraft for global-
scale sampling of the atmosphere, with flight tracks involving continuous profiling between 0.2 and 12 km altitude. Figure 1
shows the locations of 500 mbar points for aircraft profiles flown on these 4 campaigns. The majority of these profiles are
85   located over remote ocean.

There were two different PAN instruments flown on the ATom campaigns. The Georgia Tech Chemical Ionization Mass
Spectrometer (GT-CIMS) (Huey et al., 2007) was flown on ATom-2, ATom-3 and ATom-4, but not on the ATom-1 campaign.
The PAN and Trace Hydrohalocarbon ExpeRiment (PANTHER) (Elkins et al., 2001; Wofsy et al., 2011) uses electron capture
90   detection and gas chromatography to measure PAN and was flown on ATom-1, -2, -3 and -4. Figure 2 and Figure 3 show
"curtains" of PAN profile measurements from the two instruments. For the purposes of these figures, the aircraft profiles have
been split by longitude into "Pacific" (Region 1, longitude < -60°) and "Atlantic (Region 2, longitude > -60°). It can be seen
from this figure that the two instruments show a consistent picture of the large-scale PAN distribution. However, there are
some differences between the PAN measurements from the two aircraft instruments. The PANTHER values are systematically
95   higher than those from the GT-CIMS. These differences are discussed further in Section 4.

Atmospheric
Measurement
Techniques

EGU

Discussions

3 CrIS PAN retrievals

3.1 Retrieval algorithm and strategy

The single footprint CrIS PAN retrievals shown in this work were produced using the MUlti-SpEctra, MUlti-SpEcies, MUlti-Sensors (MUSES) retrieval algorithm (Fu et al., 2013, 2016, 2018; Worden et al., 2019). MUSES utilizes an optimal estimation

100   approach with a priori constraints (Rodgers, 2000) and has heritage in the TES retrieval algorithm (Bowman et al. 2006). The forward model used within MUSES for this work is the Optimal Spectral Sampling (OSS) fast radiative transfer model (Moncet et al., 2008, 2015). We use OSS v1.2, trained using the Line By Line Radiative Transfer Model (LBLRTM) v12.4 (Clough et al., 2005; Alvarado et al., 2013).

105   Provided that the retrieved state is close to the true state, the retrieved state can be expressed as:

$$\hat{\mathbf{x}}_a = \mathbf{x}_a + \mathbf{A}(\mathbf{x} - \mathbf{x}_a) + \mathbf{Gn} + \mathbf{GK}_b(\mathbf{b} - \mathbf{b}_a) + \mathbf{G}\Delta\mathbf{f} \,, \qquad (1)$$

where $\hat{\mathbf{X}}$, $\mathbf{x}_a$, and $\mathbf{x}$ are the retrieved, a priori, and the "true" state vectors. For the TES trace gas retrievals, the state vectors were expressed as the natural logarithm of volume mixing ratio (VMR). The gain matrix, $\mathbf{G}$, maps from radiance space into

110   profile space. The vector $\mathbf{n}$ is the noise on the spectral radiances. The vector $\mathbf{b}$ represents the true state for parameters that affect the modelled radiance but are not included in the retrieval state vector (such as calibration, concentrations of interfering gases, etc.). The vector $\mathbf{b}_a$ holds the corresponding a priori values. The Jacobian, $\mathbf{K}_b = \partial\mathbf{L}/\partial\mathbf{b}$, describes the sensitivity of the forward modelled radiances $\mathbf{L}$ to the vector $\mathbf{b}$. The vector $\Delta\mathbf{f}$ represents the error in the forward model relative to the true physics. Spectroscopic errors would be one component of the forward model error.

115

The averaging kernel, $\mathbf{A}$, describes the sensitivity of the retrieved state to the true state:

$$\mathbf{A} = \frac{\delta\hat{\mathbf{x}}}{\delta\mathbf{x}} = (\mathbf{K}^T\mathbf{S}_n^{-1}\mathbf{K} + \mathbf{R})^{-1}\mathbf{K}^T\mathbf{S}_n^{-1}\mathbf{K} = \mathbf{GK} \qquad (2)$$

Here, $\mathbf{K}$ is the sensitivity of the forward modeled radiances to the state vector

120   ($\mathbf{K} = \frac{\delta\mathbf{L}}{\delta\hat{\mathbf{x}}}$). The noise covariance matrix, $\mathbf{S}_n$, represents the noise in the measured radiances. $\mathbf{R}$ is the constraint matrix for the retrieval.

For profile retrievals, the widths of the rows of $\mathbf{A}$ provide a measure of the vertical resolution of the retrieval. Provided that the retrieval is relatively linear, the sum of each row of $\mathbf{A}$ indicates the fraction of retrieval information that comes from the

125   measurement as opposed to the a priori at a given altitude (Rodgers, 2000). ("Relatively linear" means that although the retrieval problem itself is non-linear (and requires iteration to reach a solution), a linearization about some prior state is

adequate to find a solution.) The trace of the averaging kernel matrix gives the number of degrees of freedom for signal (DOFS), or independent pieces of information, for the retrieval.

130   We use the PAN feature centred around 790 cm^{-1}. Figure 4 shows the PAN signal as seen in CrIS brightness temperatures for an example case from ATom-1. The microwindows used in the PAN retrievals are highlighted in red in Figure 4(b). The main interferents overlapping with the PAN feature are water vapor (H_2O), carbon dioxide (CO_2), ozone (O_3) and carbon tetrachloride (CCl_4). The retrieval windows have been chosen to avoid the strong H_2O line at 784.5 cm^{-1}, the complex of strong H_2O lines at 790-801 cm^{-1}, the CO_2 Q-branch at 791.5 cm^{-1} and the peak of the CCL_4 absorption. PAN retrievals are performed

135   after previous steps to fit surface and atmospheric temperature, surface emissivity, H_2O, O_3 and cloud optical depth and cloud top pressure. The CrIS PAN retrievals are performed in linear, rather than logarithmic volume mixing ratio.

CrIS PAN retrievals are being processed routinely under the NASA Tropospheric Ozone and Precursors from Earth System Sounding (TROPESS) project and are publicly available via the GES DISC. The TROPESS datasets at the GES DISC include the forward stream (Bowman, 2021). The TROPESS CrIS forward stream data are subsampled using a grid sampling

140   approach where the region is divided into 0.8 degree lat x 0.8 degree lon grid boxes and the single, center-most target within each box is selected to be included in the dataset. The forward stream dataset provides both day and night time coverage. Figure 5 shows a global map of CrIS PAN for an example day, using this type of grid box subsampling. The map shows colored points for retrievals that pass quality screening. Retrievals were not processed for latitudes south of 70S. There are noteable gaps in coverage over desert areas. These areas are screened out due to the presence of a strong silicate feature in

145   the surface emissivity spectrum that happens to coincide with the 790 cm^{-1} PAN feature. There are also gaps in coverage associated with strongly cloudy regions. The TROPESS datasets also include so-called "special collections" where the sampling may be tailored to address a particular scientific study (or studies). Data for this work were processed specifically for matches with ATom aircraft profiles (see Section 4).

3.2 Initial guess and a priori constraints

150   The CrIS PAN retrievals presented here use the same a priori constraint vectors as the TES PAN retrievals, as described in Payne et al. (2014). We use a monthly-varying prior constraint, constructed using a GEOS-Chem v9.01.01 global chemical transport model simulation, as described in detail in Fischer et al. (2014). There are six possible constraint vectors for any given month, based on whether the location is in or outside the Tropics and whether the model predicts "clean", 'enhanced, maximum at surface" or "enhanced, maximum aloft" for a given location. The a priori constraint matrix differs from that

155   described in Payne et al. (2014), since the TES v7 PAN retrieval is performed in ln(vmr). The constraint is loose in the troposphere and tighter in the stratosphere. We have chosen to use a diagonal constraint. For nadir retrievals, where vertical information is limited, it is common practice to introduce off-diagonal elements in the constraint matrix in order to avoid spurious oscillations in the retrieved profile. However, for fitting the broad PAN spectral feature, we did not find it necessary

to introduce off-diagonal elements in the constraint matrix. The initial guess profile values for these CrIS PAN retrievals are
160   set to a vanishingly small number.

3.2 Vertical sensitivity

The CrIS PAN retrievals are primarily sensitive to variations in PAN in the free troposphere, with greatest sensitivity in the
800 to 300 hPa vertical range. The DOFS for the CrIS PAN retrievals are generally less than 1.0, which means that the retrievals
do not provide information on the vertical distribution of PAN. We choose to retrieve PAN on multiple levels in order to
165   preserve information that the averaging kernels provide about vertical sensitivity for individual soundings, but collapse to a
single quantity per sounding for the purposes of presenting retrieved PAN values. Results are presented here in terms of a
pressure-weighted average of the retrieved PAN between 800 hPa and 300 hPa.

4 Results

The averaging kernels for the CrIS PAN retrieval are broad in vertical extent. Therefore, for the comparisons between CrIS
170   and ATom PAN observations, we selected only the aircraft profiles that span at least the 800 to 300 hPa pressure range. GEOS-
Chem model output for runs specific to the time period was appended above the uppermost and below the lowermost altitudes
spanned by these ATom PAN profiles. The GEOS-Chem runs used for this purpose were version 12.0.0, 2x2.5 degree
resolution, GEOS-FP meteorology. GEOS-Chem 12.0.0 uses the Community Emissions Database (CEDS; Hoesly et al., 2018)
as a global base case for anthropogenic emissions, overwritten with a series of local emissions inventories where appropriate:
175   in Asia (MIX; Li et al., 2017), the United States (2011 NEI; US EPA, 2015), Europe (EMEP; EMEP, 2015; Vestreng & Klein,
2002), and Africa (DICE; Marais & Wiedinmyer, 2016). Biomass burning emissions are from the Global Fire Emissions
Database (GFED) version 4 (Giglio et al., 2013), while biogenic emissions are from the Model of Emissions of Gases and
Aerosols from Nature (MEGAN) V2.1 (Guenther et al., 2012).

We used coincidence criteria of 9 hours and 50 km to match CrIS FOVs to the aircraft profiles. The CrIS PAN retrievals were
180   screened to exclude soundings with poor fits to observed radiances. In addition, we only included cases here where there were
at least 5 CrIS FOVs that match with a given aircraft profile and pass the retrieval quality screening. For the CrIS-PANTHER
comparisons, 337 aircraft profiles were considered in total for all four campaigns, with the number of good CrIS matches per
aircraft profile ranging from 5 to 72 (median of 20). For the CrIS-GTCIMS comparisons, 239 aircraft profiles were considered
185   in total for the three available campaigns, with the number of good CrIS matches per aircraft profile ranging from 5 to 67
(median of 20).

For each of the aircraft profiles, we applied the retrieval prior and averaging kernel for each of the individual matched CrIS
FOVs to the appended aircraft profiles to calculate a "convolved aircraft profile" for each FOV, representing what we would

190   expect from the satellite retrieval if the appended aircraft profile represented the true atmospheric state viewed by the satellite. We then calculate a pressure-weighted average between 800 and 300 hPa for each convolved aircraft profile for comparison with the CrIS results.

A linear fit of the GT-CIMS-based vertical averages (from the "convolved" profiles) to those from the PANTHER (for the

195   239 profiles where both datasets were available) results in a gradient of 0.86 and a negligible intercept. The R^2 value for the linear fit is 0.92, indicating that while there there is a systematic difference between the two sets of aircraft measurements, they are very strongly correlated. The scatter around the fitted line for this comparison of GT-CIMS/PANTHER vertical averages is around 0.015 ppbv. The mean difference between the two sets of values is 0.007 ppbv (most of the aircraft measurements are at the low end of the range).

200

Figure 6 shows CrIS-PANTHER differences plotted by latitude for each of the 4 campaigns and Figure 7 shows the CrIS-PANTHER comparisons in a scatter plot. The CrIS points in Figure 7 correspond to the "averages for each aircraft profile" shown in Figure 6. The R^2 value between CrIS and PANTHER values (all 4 campaigns) is 0.61. The R^2 value between the retrieval prior and the PANTHER values is 0.38. (For the GT-CIMS dataset from ATom 2, 3, and 4, the R^2 value between

205   CrIS and aircraft is 0.64 and the R^2 value between prior and aircraft is 0.53.) A summary of the mean bias and standard deviation of CrIS-aircraft comparison results is provided in Table 1 for both the PANTHER and GT-CIMS aircraft measurements. The standard deviation of the CrIS-aircraft comparisons for individual CrIS soundings is 0.08 ppbv (for both aircraft datasets). This suggests that 0.08 ppbv is a reasonable estimate for the uncertainty on a single CrIS PAN retrieval. The standard deviation of the CrIS-aircraft comparisons for averaged CrIS retrievals (multiple satellite co-incidences with each

210   aircraft profile) is lower, at 0.05 ppbv. This would suggest that the retrieval error reduces with averaging, although not with the square root of the number of observations.

The optimal estimation approach used within the MUSES algorithm provides an estimate of the observation error as part of the retrieval output. Comparisons between the values of this estimated observation error for individual soundings and the

215   standard deviation of the CrIS-aircraft comparisons for individual CrIS soundings (empirical observation error) indicate that the estimated errors output from the optimal estimation retrieval are too low by a factor of 2-3. Therefore, we recommed using the empirical value of 0.08 ppbv as an estimate of uncertainty on individual soundings rather than the observation errors reported for the retrievals.

220   Since the uncertainties on the CrIS PAN retrievals are large compared to those on the aircraft measurements, the differences between the aircraft datasets do not affect the conclusions about the CrIS PAN retrieval uncertainties and the magnitude of the bias in the CrIS PAN. The results demonstrate overall consistency between CrIS-PANTHER results for the four separate campaigns and between the CrIS-PANTHER and CrIS-GTCIMS results, and the CrIS PAN retrievals show skill relative to

the monthly climatology used for the retrieval prior (increased R^2 value for a linear fit to the aircraft values) whether the

225 PANTHER or GT-CIMS aircraft dataset is used.

Table 1. Mean and standard deviation of CrIS-aircraft differences, by instrument and campaign

ATom campaign (dates)	CrIS-PANTHER PAN [ppbv]				CrIS-GTCIMS PAN [ppbv]			
	Individual CrIS		Averaged CrIS		Individual CrIS		Averaged CrIS	
	Mean	Std. dev.	Mean	Std. dev.	Mean	Std. dev.	Mean	Std. dev.
ATom 1 July-August 2016	-0.09	0.09	-0.10	0.06	n/a	n/a	n/a	n/a
ATom 2 January-February 2017	-0.09	0.08	-0.09	0.06	-0.08	0.08	-0.08	0.06
ATom 3 September-October 2017	-0.06	0.07	-0.05	0.04	-0.06	0.08	-006	0.05
ATom 4 April-May 2018	-0.09	0.08	-0.09	0.06	-0.07	0.09	-0.07	0.06
All	-0.08	0.08	-0.08	0.05	-0.07	0.08	-0.07	0.05

5 Discussion and Conclusions

We have developed an algorithm for retrieval of PAN from single field of view L1B CrIS radiances and have validated results

230 against two sets of aircraft profile measurements from ATom. The CrIS PAN retrievals are primarily sensitive in the mid-troposphere and have 1.0 or fewer DOFs, meaning that they do not provide information on the vertical distribution of PAN. We show results in terms of a single vertically averaged quantity. We find a negative bias of order 0.1 ppbv in the CrIS PAN results with respect to the aircraft measurements. This bias does not appear to show a dependence on latitude or season. We also find good consistency between results from the four different ATom campaigns. Based on this study, we expect this bias

235 to apply to all parts of the world. For the future, more validation data over land would be desirable. For remote regions, the observed bias is large relative to absolute PAN values, although it would be a smaller fraction of the absolute PAN values in fire plumes, for example. The results suggest a single sounding uncertainty of around 0.08 ppbv, and demonstrate the ability of the CrIS PAN retrievals to capture variation in the "background" PAN values observed over remote ocean regions from ATom. For demonstration of the capability of CrIS to capture PAN in fire plumes, we refer to recent work by Juncosa

240 Calahorrano et al. (2021).

Acknowledgements

Data availability

250   The ATom aircraft datasets were obtained from https://doi.org/10.3334/ORNLDAAC/1581 (Wofsy et al., 2018). MUSES-CrIS PAN products from S-NPP and JPSS-1 are available via the GES-DISC from the NASA Tropospheric Ozone and Precursors from Earth System Sounding (TROPESS) project at https://disc.gsfc.nasa.gov/datasets/TRPSDL2PANCRSFS_1/summary and https://disc.gsfc.nasa.gov/datasets/TRPSDL2PANCRS1FS_1/summary respectively. The CrIS – aircraft matched dataset

255   used here for validation is available from the authors on request.

Author contributions

VHP, SSK and EVF were responsible for study design. VHP and SSK were responsible for algorithm development, data analysis and manuscript writing. JFB was responsible for GEOS-Chem runs for the ATom time periods. LGH, SCW, JE, EH,

260   FM and EVF were responsible for providing aircraft measurements and guidance on their use. KM and JJC contributed to overall assessment of the CrIS data quality and manuscript editing. JRW contributed to the interpretation of validation results. JRW and KWB are responsible for data dissemination via management of the TROPESS project.

References

265   Alvarado, M. J., J. A. Logan, J. Mao, E. Apel, D. Riemer, D. Blake, R. C. Cohen, K. E. Min, A. E. Perring, E. C. Browne, P. J. Wooldridge, G. S. Diskin, G. W. Sachse, H. Fuelberg, W. R. Sessions, D. L. Harrigan, G. Huey, J. Liao, A. Case-Hanks, J. L. Jimenez, M. J. Cubison, S. A. Vay, A. J. Weinheimer, D. J. Knapp, D. D. Montzka, F. M. Flocke, I. B. Pollack, P. O. Wennberg, A. Kurten, J. Crounse, J. M. S. Clair, A. Wisthaler, T. Mikoviny, R. M. Yantosca, C. C. Carouge, and P. Le

Atmospheric
Measurement
Techniques
Open Access
EGU
Discussions

Sager (2010), Nitrogen oxides and PAN in plumes from boreal fires during ARCTAS-B and their impact on ozone: an

270   integrated analysis of aircraft and satellite observations, *Atmos. Chem. Phys.*, *10*(20), 9739-9760,10.5194/acp-10-9739-2010.

Alvarado, M. J., Cady-Pereira, K. E., Xiao, Y., Millet, D. B. and Payne, V. H.: Emission Ratios for Ammonia and Formic Acid and Observations of Peroxy Acetyl Nitrate (PAN) and Ethylene in Biomass Burning Smoke as Seen by the Tropospheric Emission Spectrometer (TES), Atmosphere 2, 633-654, 2011

275

Alvarado, M.J., V.H. Payne, E.J. Mlawer, G. Uymin, M.W. Shephard, K.E. Cady-Pereira, J.S. Delamere, and J.L. Moncet (2013), Performance of the Line-By-Line Radiative Transfer Model (LBLRTM) for temperature, water vapor, and trace gas retrievals: recent updates evaluated with IASI case studies, *Atmos. Chem. Phys.*, *13*, 6687-6711, doi:10.5194/acp-13-6687-2013.

280

Bowman, K. W., Rodgers, C. D., Sund-Kulawik, S., Worden, J., Sarkissian, E., Osterman, G., Steck, T., Luo, M., Eldering, A., Shephard, M. W., Worden, H., Clough, S. A., Brown, P. D., Rinsland, C. P., Lampel, M., Gunson, M., and Beer, R.: Tropospheric emission spectrometer: Retrieval method and error analysis, IEEE Geosci. Remote Sens., 44(5), 1297–1307, doi:10.1109/TGRS.2006.871234, 2006.

285

Bowman, K. W. (2021), TROPESS CrIS-SNPP L2 Peroxyacytyl Nitrate for Forward Stream, Standard Product V1, Greenbelt, MD, USA, Goddard Earth Sciences Data and Information Services Center (GES DISC), Accessed: 18th August 2021, 10.5067/MQITF51HVPNW

290   Clarisse, L., R'Honi, Y., Coheur, P.-F., Hurtmans, D. and Clerbaux, C.: Thermal infrared nadir observations of 24 atmospheric gases. *Geophys. Res. Lett*, *38,* doi:10.1029/2011GL047271, 2011.
Fiore, A. M., E. V. Fischer, S. Pandey Deolal, O. Wild, D. Jaffe, J. Staehelin, O. E. Clifton, G. P. Milly, D. Bergmann, W. Collins, F. Dentener, R. M. Doherty, B. N. Duncan, B. Fischer, S. Gilge, P. G. Hess, L. W. Horowitz, A. Lupu, I. MacKenzie, R. Park, L. Ries, M. Sanderson, M. G. Schultz, D. T. Shindell, M. Steinbacher, D. S. Stevenson, S. Szopa, C.
295   Zellweger, and G. Zeng (2018), Regional and intercontinental pollution signatures on modeled and measured PAN at northern mid-latitude mountain sites, *Atmos. Chem. Phys. Discuss.*, *2018*, 1-38,10.5194/acp-2018-90.

Elkins, J. W., Moore, F. L., and Kline, E. S.: Next Generation Airborne Gas chromatograph for NASA Airborne Platforms, Earth Science Technology Conference 2001, 28–30 August 2001, College Park, MD, 2001.

300   EMEP, Co-operative programme for monitoring and evaluation of long-range transmission of air pollutants in Europe, Status report (2015), https://emep.int/publ/reports/2015/EMEP_Status_Report_1_2015.pdf, ISSN 1504-6192

Fischer, E. V., D. J. Jacob, R. M. Yantosca, M. P. Sulprizio, D. B. Millet, J. Mao, F. Paulot, H. B. Singh, A. Roiger, L. Ries, R. W. Talbot, K. Dzepina, and S. Pandey Deolal (2014), Atmospheric peroxyacetyl nitrate (PAN): a global budget and source attribution, *Atmos. Chem. Phys.*, *14*(5), 2679-2698,10.5194/acp-14-2679-2014.

305

Fischer, E. V., Zhu, L., Payne, V. H., Worden, J. R., Jiang, Z., Kulawik, S. S., Brey, S., Hecobian, A., Gombos, D., Cady-Pereira, K., and Flocke, F.: Using TES retrievals to investigate PAN in North American biomass burning plumes, Atmos. Chem. Phys., 18, 5639-5653, https://doi.org/10.5194/acp-18-5639-2018, 2018.

310   Franco, B., Clarisse, L., Stavrakou, T., Mueller, J-F., Van Damme, M., Whitburn, S., Hadji-Lazaro, J., Hurtmans, D., Taraborelli, D., Clerbaux, C. and Coheur, P-F.: A General Framework for Global Retrievals of Trace Gases from IASI: Application to Methanol, Formic Acid and PAN, J. Geophys. Res. Atmos., 123, 13963-13984, doi:10.1029/2018JD029633, 2018.

315   Fu, D., Worden, J. R., Liu, X., Kulawik, S. S., Bowman, K. W., and Natraj, V.: Characterization of ozone profiles derived from Aura TES and OMI radiances, Atmos. Chem. Phys., 13, 3445-3462, https://doi.org/10.5194/acp-13-3445-2013, 2013.

Fu, D., Bowman, K. W., Worden, H. M., Natraj, V., Worden, J. R., Yu, S., Veefkind, P., Aben, I., Landgraf, J., Strow, L., and Han, Y.: High-resolution tropospheric carbon monoxide profiles retrieved from CrIS and TROPOMI, Atmos. Meas. Tech., 9, 320   2567-2579, https://doi.org/10.5194/amt-9-2567-2016, 2016.

Fu, D., Kulawik, S. S., Miyazaki, K., Bowman, K. W., Worden, J. R., Eldering, A., Livesey, N. J., Teixeira, J., Irion, F. W., Herman, R. L., Osterman, G. B., Liu, X., Levelt, P. F., Thompson, A. M., and Luo, M.: Retrievals of tropospheric ozone profiles from the synergism of AIRS and OMI: methodology and validation, Atmos. Meas. Tech., 11, 5587-5605, 325   https://doi.org/10.5194/amt-11-5587-2018, 2018.

Fu, D., Millet, D. B., Wells, K., Payne, V. H., Yu, S., Guenther, A. and Eldering, A.: Direct measurements of isoprene from infrared satellite observations, Nature Communications, 10, Article number 3811, https://doi.org/10.1038/s41467-019-11835-0, 2019

330

Giglio, L., Randerson, J. T., and van der Werf, G. R., (2013), Analysis of daily, monthly, and annual burned area using the fourth-generation global fire emissions database (GFED4) *J. Geophys. Res. Biogeosci.*, 118, 317– 328, doi:10.1002/jgrg.20042

335 Guenther, A. B., Jiang, X., Heald, C. L., Sakulyanontvittaya, T., Duhl, T., Emmons, L. K., and Wang, X.: The Model of Emissions of Gases and Aerosols from Nature version 2.1 (MEGAN2.1): an extended and updated framework for modeling biogenic emissions, Geosci. Model Dev., 5, 1471–1492, https://doi.org/10.5194/gmd-5-1471-2012, 2012.

Han, Y., Revercomb, H., Cromp, M., Gu, D., Johnson, D., Mooney, D., Scott, D., Strow, L., Bingham, G., Borg, L., Chen, Y.,
340 DeSlover, D., Esplin, M., Hagan, D., Jin, X., Knuteson, R., Motteler, H., Predina, J., Suwinski, L., Taylor, J., Tobin, D., Tremblay, D., Wang, C., Wang, L., Wang, L. and Zavylov, V.: Suomi-NPP CrIS measurements, sensor data record algorithm, calibration and validation activities and record data quality, J. Geophys. Res. Atmos., 118, 1-15, doi:10.1002/2013JD020344, 2013

345 Hoesly, R. M., Smith, S. J., Feng, L., Klimont, Z., Janssens-Maenhout, G., Pitkanen, T., Seibert, J. J., Vu, L., Andres, R. J., Bolt, R. M., Bond, T. C., Dawidowski, L., Kholod, N., Kurokawa, J.-I., Li, M., Liu, L., Lu, Z., Moura, M. C. P., O'Rourke, P. R., and Zhang, Q.: Historical (1750–2014) anthropogenic emissions of reactive gases and aerosols from the Community Emissions Data System (CEDS), Geosci. Model Dev., 11, 369–408, https://doi.org/10.5194/gmd-11-369-2018, 2018.

350 Huey, L. G.: Measurement of trace atmospheric species by chemical ionization mass spectrometry: Speciation of reactive nitrogen and future directions, *Mass Spectrom Rev., 26*, 166-184, 2007

Juncosa Calahorrano, J., Payne, V. H., Kulawik, S. S., Flocke, F., Campos, T., and Fischer, E. V.: Evolution of PAN in wildfire smoke plumes detected by the Cross-Track Infrared Sounder (CrIS) over the western US during summer 2018,
355 accepted for publication in Geophys. Res. Lett., 2021

Li, M., Zhang, Q., Kurokawa, J.-I., Woo, J.-H., He, K., Lu, Z., Ohara, T., Song, Y., Streets, D. G., Carmichael, G. R., Cheng, Y., Hong, C., Huo, H., Jiang, X., Kang, S., Liu, F., Su, H., and Zheng, B.: MIX: a mosaic Asian anthropogenic emission inventory under the international collaboration framework of the MICS-Asia and HTAP, Atmos. Chem. Phys., 17, 935–963,
360 https://doi.org/10.5194/acp-17-935-2017, 2017.

Mahieu, E., Fischer, E. V., Franco, B., Palm, M., Wizenberg, T., Smale, D., Clarisse, L., Clerbaux, C., Coheur, P-F., Hannigan, J. W., Lutsch, E., Notholt, J., Pardo Cantos, I., Prignon, M., Servais, C., and Strong, K.; First retrievals of peroxyacetyl nitrate (PAN) from ground-based FTIR solar spectra recorded at remote sites, comparison with model and
365 satellite data. *Elementa: Science of the Anthropocene* 21 January 2021; 9 (1): 00027.
doi: https://doi.org/10.1525/elementa.2021.00027

Marais, E. A. and Wiedinmyer, C, Air Quality Impact of Diffuse and Inefficient Combustion Emissions in Africa (DICE-Africa), *Environ. Sci. Tech.*, 50, 10739-10745, 2016, doi:10.1021/acs.est.6b02602.

370

Moncet, J-L., Uymin, G., Liang, P. and Lipton, A. E.: Fast and accurate radiative transfer in the thermal regime by simultaneous optimal spectral sampling over all channels, J. Atmos, Sci., doi:10.1175/JAS-D-14-0190, 2015

Moncet, J.-L., Uymin, G., Lipton, A. E. and Snell, H. E.: Infrared radiance modeling by optimal spectral sampling. *J. Atmos.*

375   *Sci.*, **65**, 3917–3934, doi:10.1175/2008JAS2711.1, 2008

Moore, D. P., and Remedios, J. J.: Seasonality of Peroxyacetyl nitrate (PAN) in the upper troposphere and lower stratosphere using the MIPAS-E instrument, Atmos. Chem. Phys., 10(13), 6117-6128. doi:10.5194/acp-10-6117-2010, 201
Pollack, I. B., T. B. Ryerson, M. Trainer, J. A. Neuman, J. M. Roberts, and D. D. Parrish (2013), Trends in ozone, its

380   precursors, and related secondary oxidation products in Los Angeles, California: A synthesis of measurements from 1960 to 2010, *Journal of Geophysical Research: Atmospheres*, *118*(11), 5893-5911,doi:10.1002/jgrd.50472.

Pope, R. J., Richards, N. A. D., Chipperfield, M. P., Moore, D. P., Monks, S. A., Arnold, S. R., Glatthor, N., Kiefer, M.,

385   Breider, T. J., Harrison, J. J., Remedios, J. J., Warneke, C., Roberts, J. M., Diskin, G. S., Huey, L. G., Wisthaler, A., Apel, E. C., Bernath, P. F., and Feng, W.: Intercomparison and evaluation of satellite peroxyacetyl nitrate observations in the upper troposphere–lower stratosphere, Atmos. Chem. Phys., 16, 13541-13559, doi:10.5194/acp-16-13541-2016, 2016.

Revercomb, H. and Strow, L.: Suomi NPP CrIS Level 1B Full Spectral Resolution V2, Accessed from GES DISC February

390   2019, doi: 10.5067/9NPOTPIPLMAW, 2018

Roberts, J. M.: PAN and Related Compounds, in: Volatile Organic Compounds in the Atmosphere, Blackwell Publishing Ltd, 221– 268, 2007.

395   Rodgers, C. D., Inverse methods for atmospheric Sounding: Theory and Practice, World Sci., Hackensack, N. J., 2000.

Shephard, M. W. and Cady-Pereira, K. E., Cross-track Infrared Sounder (CrIS) satellite observations of tropospheric ammonia, Atmos. Meas. Tech., 8, 1323-1336, doi:10.5194/amt-8-1323-2015, 2015

400   Singh, H. B., and P. L. Hanst (1981), Peroxyacetyl nitrate (PAN) in the unpolluted atmosphere: An important reservoir for nitrogen oxides, *Geophys. Res. Lett.*, *8*(8), 941-944,10.1029/GL008i008p00941.

Singh, H., Salas, L. & Viezee, W. Global distribution of peroxyacetyl nitrate. *Nature* **321,** 588–591 (1986). https://doi.org/10.1038/321588a0

405 Tereszchuk, K. A., Moore, D. P., Harrison, J. J., Boone, C. D., Park, M., Remedios, J. J., Randel, W. J. and Bernath, P. F.: Observations of peroxyacetyl nitrate (PAN) in the upper troposphere by the Atmospheric Chemistry Experiment-Fourier Transform Spectrometer (ACE-FTS), Atmos. Chem. Phys., 13, 5601-5613, 2013

Tobin, D., Revercomb, H, Knuteson, R., Taylor, J., Best, F., Borg, L., DeSlover, D., Martin, G., Buijs, H., Esplin, M., Glumb,
410 R., Han, Y., Mooney, D., Predina, J., Strow, L., Suwinski, L. and Wang, L.: Suomi-NPP CrIS radiometric calibration uncertainty, J. Geophys. Res. Atmos., 118, 10589-10699, doi:10.1002/jgrd.50809, 2013
Wang, Y., D. J. Jacob, and J. A. Logan (1998), Global simulation of tropospheric O$_3$ - NO$_x$ - hydrocarbon chemistry: 3. Origin of tropospheric ozone and effects of nonmethane hydrocarbons, *Journal of Geophysical Research: Atmospheres*, *103*(D9), 10757-10767,doi:10.1029/98JD00156.
415

United States Environmental Protection Agency (US EPA): 2011 National Emissions Inventory data, https://www.epa.gov/air-emissions-inventories/2011-national-emissions-inventory-nei-data. Documentation updated 2015.

Wiegele, A., Glatthor, N., Hoepfner, M., Grabowski, U., Kellmann, S., Linden, A., Stiller, G. and von Clarmann, T.: Global
420 distributions of C2H6, C2H2, HCN and PAN retrieved from MIPAS reduced spectral resolution measurements, Atmos. Meas. Tech., 5, 723-734, 2012

Wofsy, S. C., et al. (2011), HIAPER Pole-to-Pole Observations (HIPPO): Fine-grained, global scale measurements of climatically important atmospheric gases and aerosols, *Philosophical Transacations of the Royal Society of London A*, 369,
425 2037-2086, doi:10.1098/rsta2010.0313

Wofsy, S.C., S. Afshar, H.M. Allen, E. Apel, E.C. Asher, B. Barletta, J. Bent, H. Bian, B.C. Biggs, D.R. Blake, N. Blake, I. Bourgeois, C.A. Brock, W.H. Brune, J.W. Budney, T.P. Bui, A. Butler, P. Campuzano-Jost, C.S. Chang, M. Chin, R. Commane, G. Correa, J.D. Crounse, P. D. Cullis, B.C. Daube, D.A. Day, J.M. Dean-Day, J.E. Dibb, J.P. DiGangi, G.S. Diskin,
430 M. Dollner, J.W. Elkins, F. Erdesz, A.M. Fiore, C.M. Flynn, K. Froyd, D.W. Gesler, S.R. Hall, T.F. Hanisco, R.A. Hannun, A.J. Hills, E.J. Hintsa, A. Hoffman, R.S. Hornbrook, L.G. Huey, S. Hughes, J.L. Jimenez, B.J. Johnson, J.M. Katich, R.F. Keeling, M.J. Kim, A. Kupc, L.R. Lait, J.-F. Lamarque, J. Liu, K. McKain, R.J. Mclaughlin, S. Meinardi, D.O. Miller, S.A. Montzka, F.L. Moore, E.J. Morgan, D.M. Murphy, L.T. Murray, B.A. Nault, J.A. Neuman, P.A. Newman, J.M. Nicely, X. Pan, W. Paplawsky, J. Peischl, M.J. Prather, D.J. Price, E. Ray, J.M. Reeves, M. Richardson, A.W. Rollins, K.H. Rosenlof,
435 T.B. Ryerson, E. Scheuer, G.P. Schill, J.C. Schroder, J.P. Schwarz, J.M. St.Clair, S.D. Steenrod, B.B. Stephens, S.A. Strode,

C. Sweeney, D. Tanner, A.P. Teng, A.B. Thames, C.R. Thompson, K. Ullmann, P.R. Veres, N. Vieznor, N.L. Wagner, A. Watt, R. Weber, B. Weinzierl, P. Wennberg, C.J. Williamson, J.C. Wilson, G.M. Wolfe, C.T. Woods, and L.H. Zeng. 2018. ATom: Merged Atmospheric Chemistry, Trace Gases, and Aerosols. ORNL DAAC, Oak Ridge, Tennessee, USA. https://doi.org/10.3334/ORNLDAAC/1581

440 Ungermann, J., Ern, M., Kaufmann, M., Müller, R., Spang, R., Ploeger, F., Vogel, B., and Riese, M.: Observations of PAN and its confinement in the Asian summer monsoon anticyclone in high spatial resolution, Atmos. Chem. Phys., 16, 8389 8403, doi:10.5194/acp-16-8389-2016, 2016.

Vestreng, V. and Klein, H.: Emission data reported to UNECE/EMEP: Quality assurance and trend analysis, MSC-W Status Report 2002 (2002), ISSN 0332-9879

445 Worden, J. R., Kulawik, S. S., Fu, D., Payne, V. H., Lipton, A. E., Polonsky, I., He, Y., Cady-Pereira, K., Moncet, J.-L., Herman, R. L., Irion, F. W., and Bowman, K. W.: Characterization and evaluation of AIRS-based estimates of the deuterium content of water vapor, Atmos. Meas. Tech., 12, 2331-2339, https://doi.org/10.5194/amt-12-2331-2019, 2019.
Zavyalov, V., Esplin, M., Scott, D., Esplin, B., Bingham, G., Hoffman, E., Lietzke, C., Predina, J., Frain, R., Suwinnski, L., Han, Y., Major, C., Graham, B. and Phillips, L.: Noise performance of the CrIS instrument, J. Geophys. Res. Atmos., 118, 450 13108-13120, doi:10.1002/2013JD020457, 2013

Zhu, L., Fischer, E. V., Payne, V. H., Worden, J. R. and Jiang, Z.:, TES observations of the interannual variability of PAN over Northern Eurasia and the relationship to springtime fires, Geophys. Res. Lett., 42, 7230–7237, doi:10.1002/2015GL065328, 2015.

455

Zhu, L., Fischer, E. V., Payne, V. H., *Walker, T. W.*, Worden, J. R., Jiang, Z. and Kulawik, S. S.: PAN in the Eastern Pacific Free Troposphere: A Satellite View of the Sources, Seasonality, Interannual Variability and Timeline for Trend Detection, J. Geophys. Res. Atmos., 122, 3614-3629, DOI:10.1002/2016JD025868, 2017.
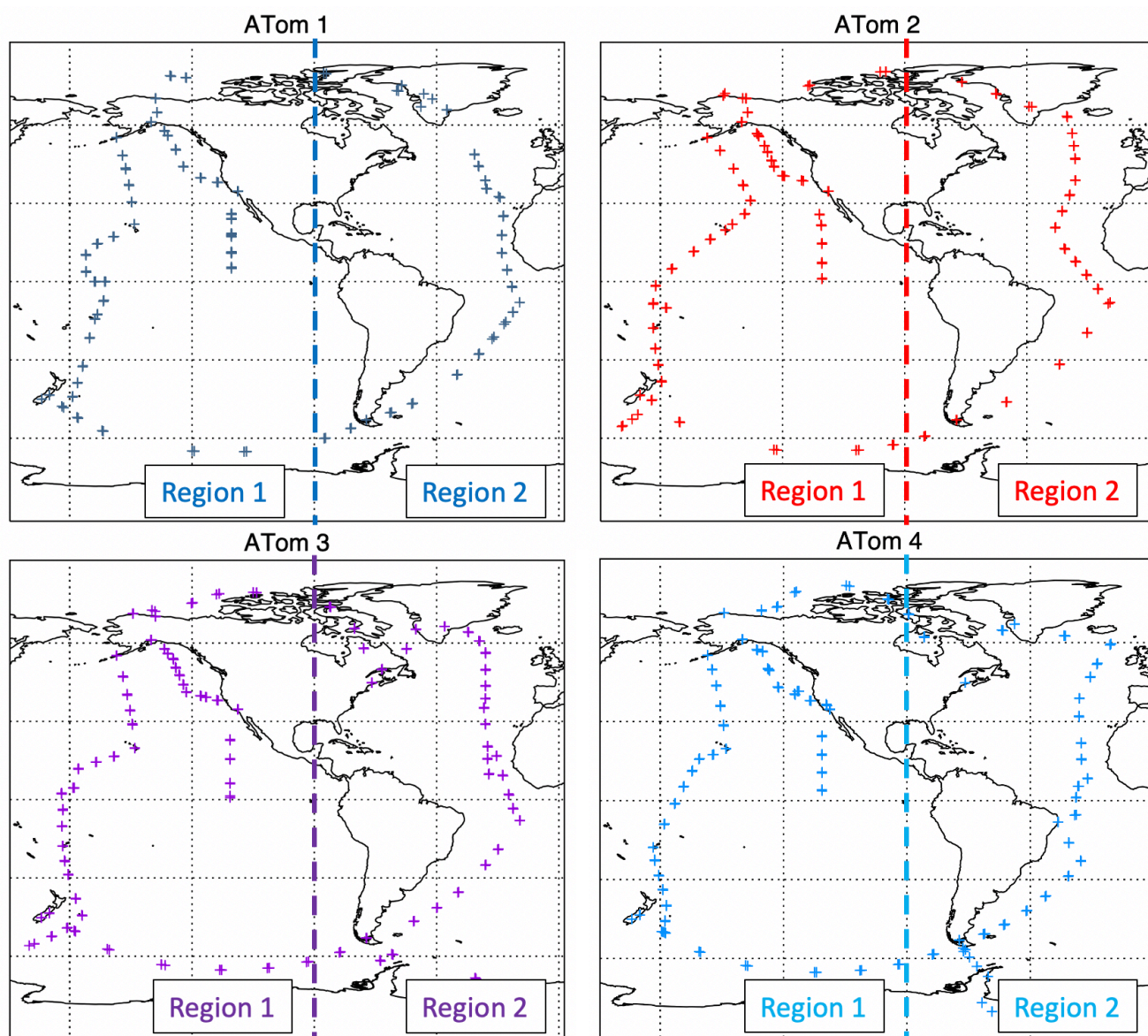
460

Figure 1. Locations of 500 mbar pressure in aircraft profiles measured during the ATom campaigns. The vertical line at 60 degrees shows the separation into "Region 1" (Pacific) and "Region 2" (Atlantic).
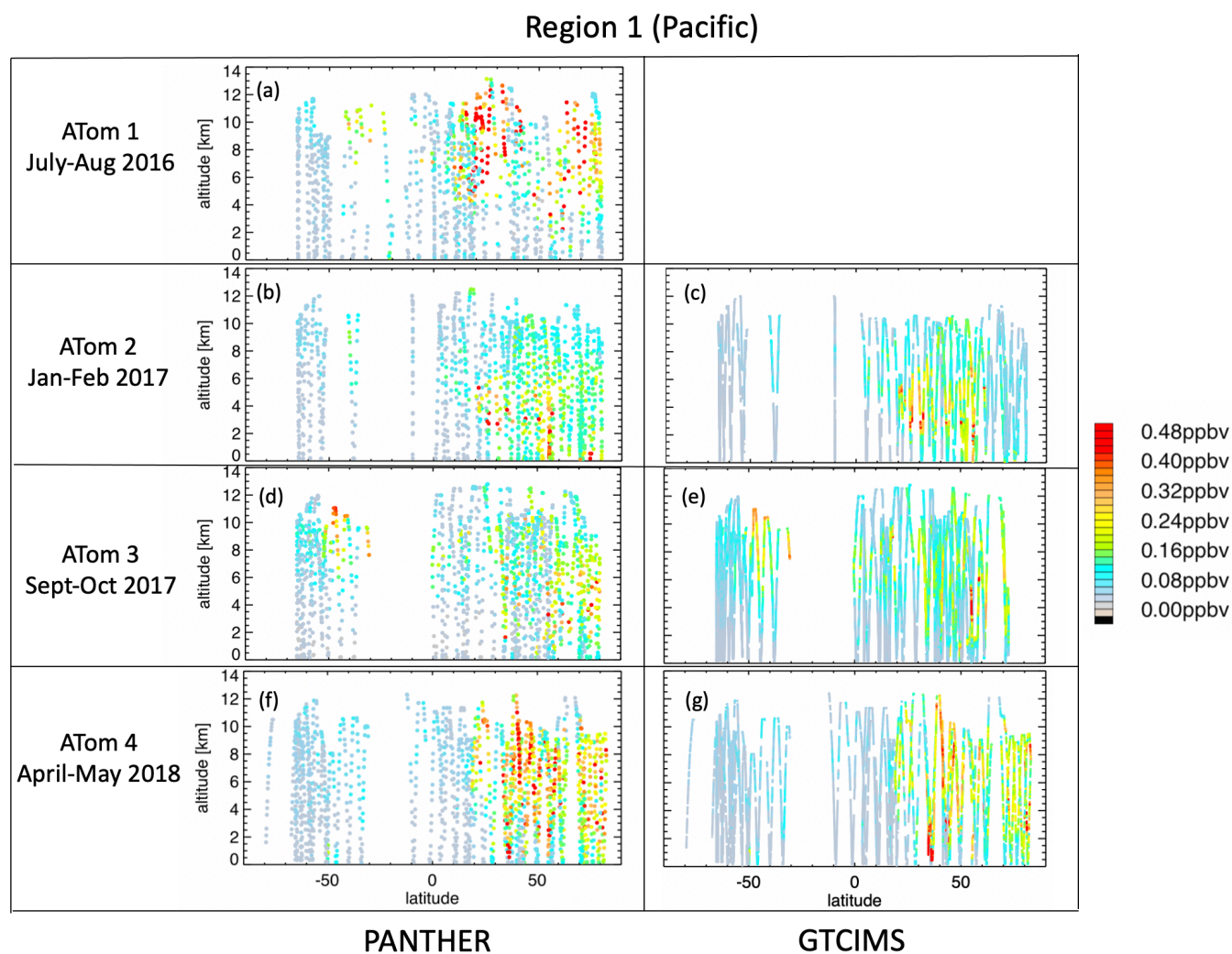
465

Figure 2. Aircraft measurements of PAN from the PANTHER (a, b, d, f) and GTCIMS (c, e, g) instruments from ATom 1, 2, 3 and 4 for Region 1 ("Pacific", longitude less than -60º).
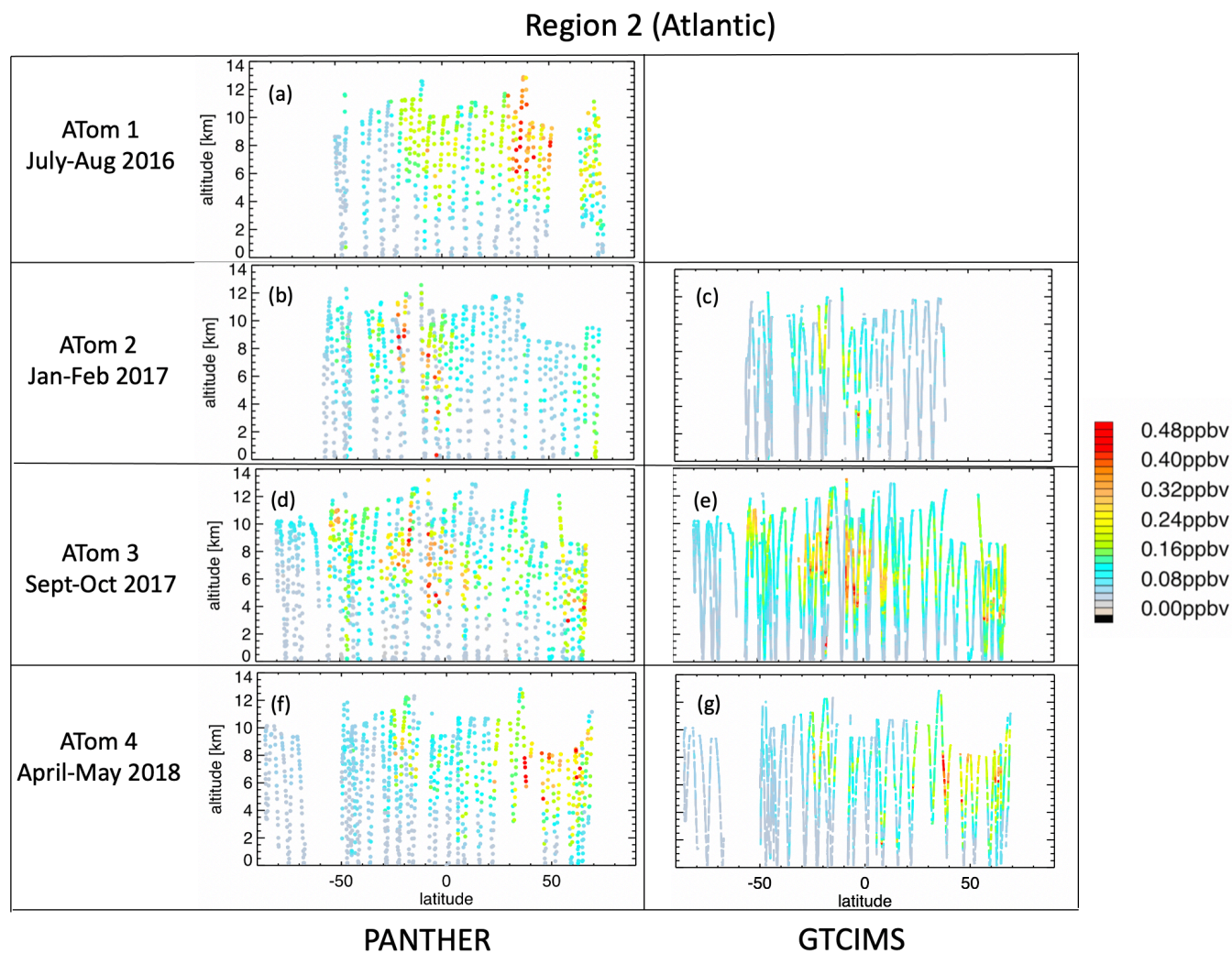
470

Figure 3. Aircraft measurements of PAN from the PANTHER (a, b, d, f) and GTCIMS (c, e, g) instruments from ATom 1, 2, 3 and 4 for Region 1 ("Atlantic", longitude greater than -60º).
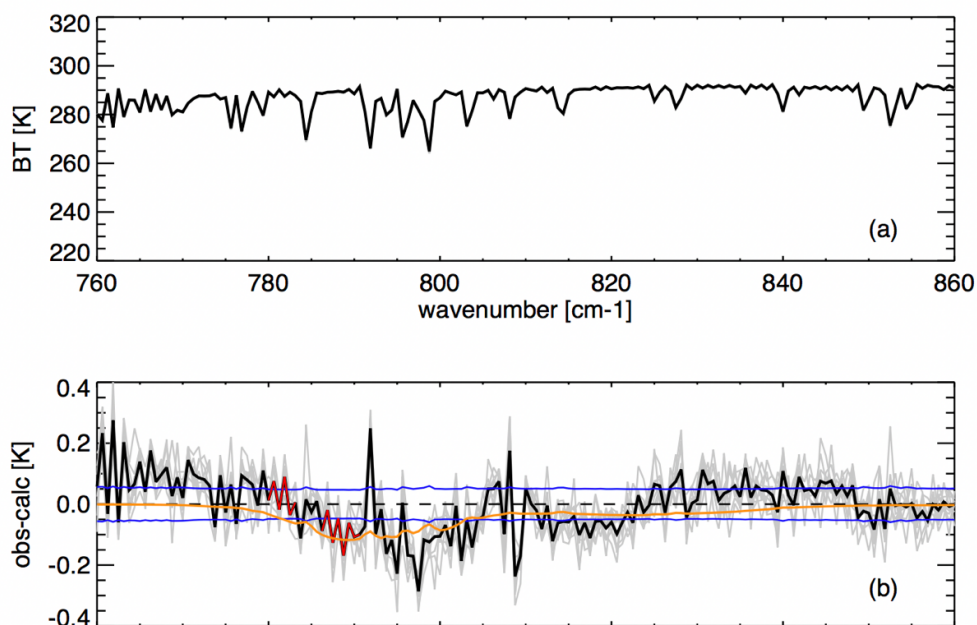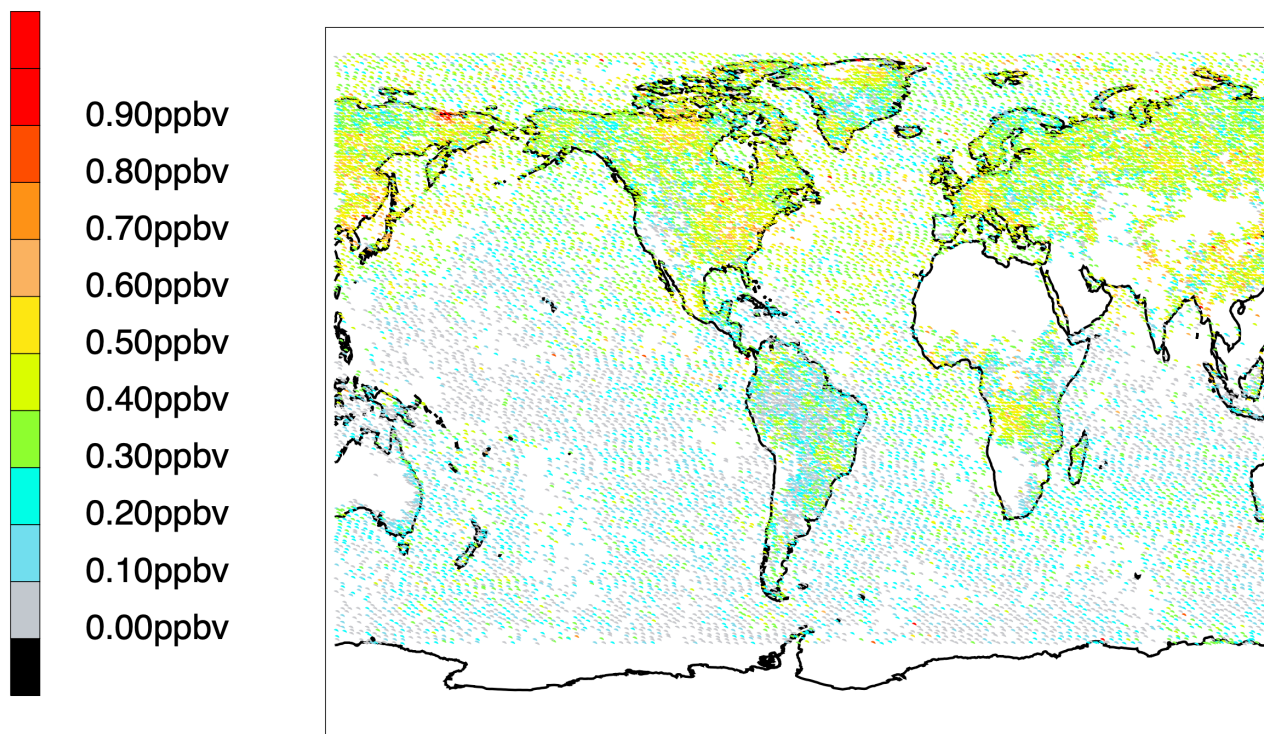
480

Figure 4: (a) Measured CrIS brightness temperature spectrum for a case co-located with an ATom-1 profile on 17th August 2016, at 36.2 degrees latitude, -27.3 degrees longitude. (b) Residual spectra (observed – calculated) for match-ups with this ATom-1 case, with zero PAN in the calculation, after retrieval of surface and atmospheric temperature, water vapor, cloud optical depth, cloud top pressure and surface emissivity. Grey lines show residuals for individual CrIS FOVs that meet the co-incidence criteria. Black
485 **line shows the mean residual for this set. Red segments show the microwindows used in the retrievals. Blue lines show the NEdT for a single CrIS FOV. Orange line shows the shape of the PAN spectral feature.**

Atmospheric
Measurement
Techniques
Discussions

Figure 5. CrIS PAN for 1st August 2020 (sub-sampled by selecting the center-most CrIS FOV in each 0.8 by 0.8 degree grid box for
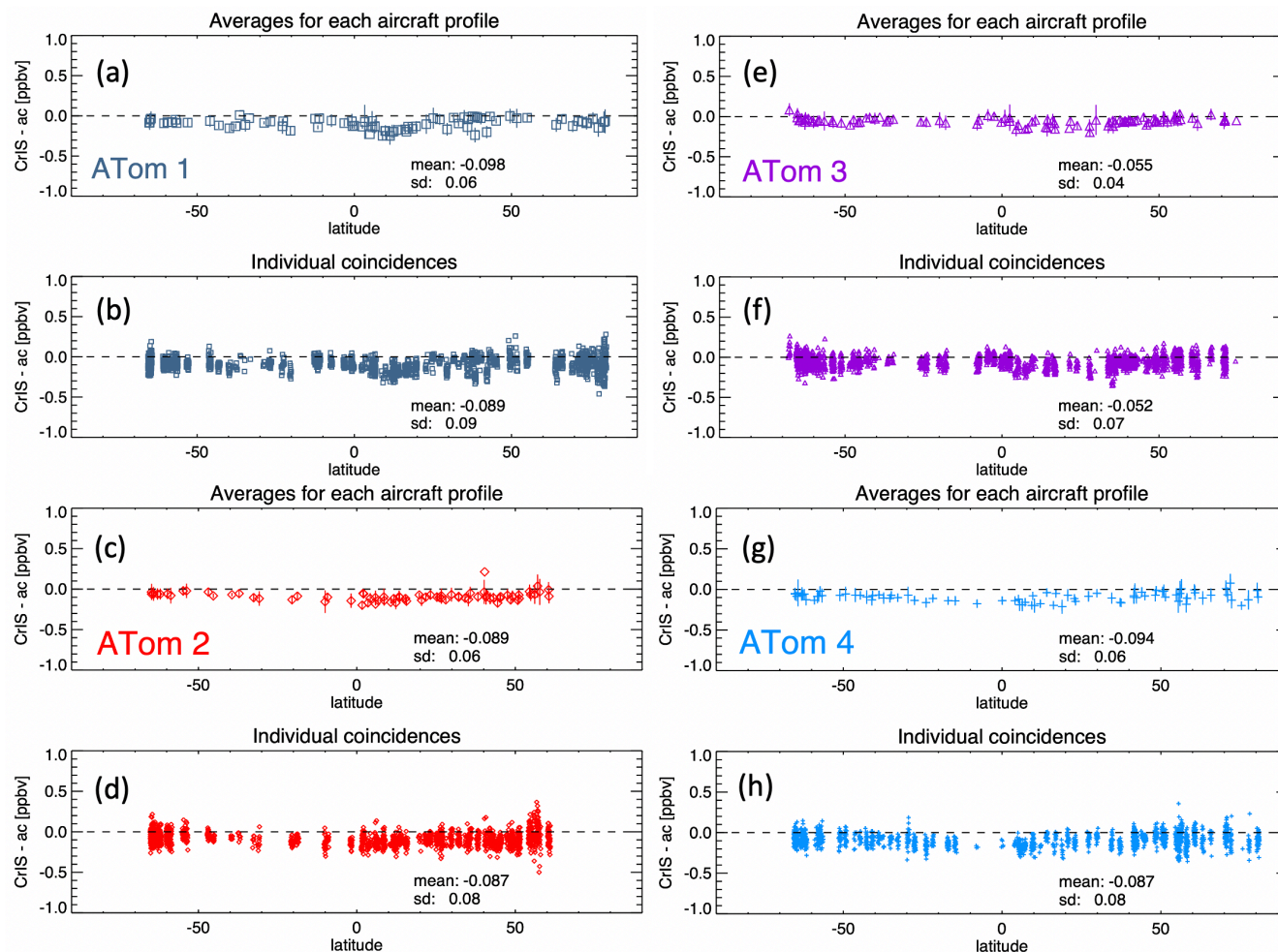490   **latitudes above 70S).**

495

Figure 6. CrIS-PANTHER PAN differences against latitude for the four ATom aircraft campaigns. Results from ATom 1 are shown in panels (a) and (b), ATom 2 in (c) and (d), ATom 3 in (e) and (f) and ATom 4 in (g) and (h). Panels (a), (c), (e) and (g) show the results after averaging all the CrIS co-incidences for each aircraft profile. Vertical bars on the points in these panels show the standard deviation of the averaged CrIS result for each aircraft profile. Panels (b), (d), f) and (h) show the results for individual CrIS soundings (multiple CrIS co-incidences with each aircraft profile.
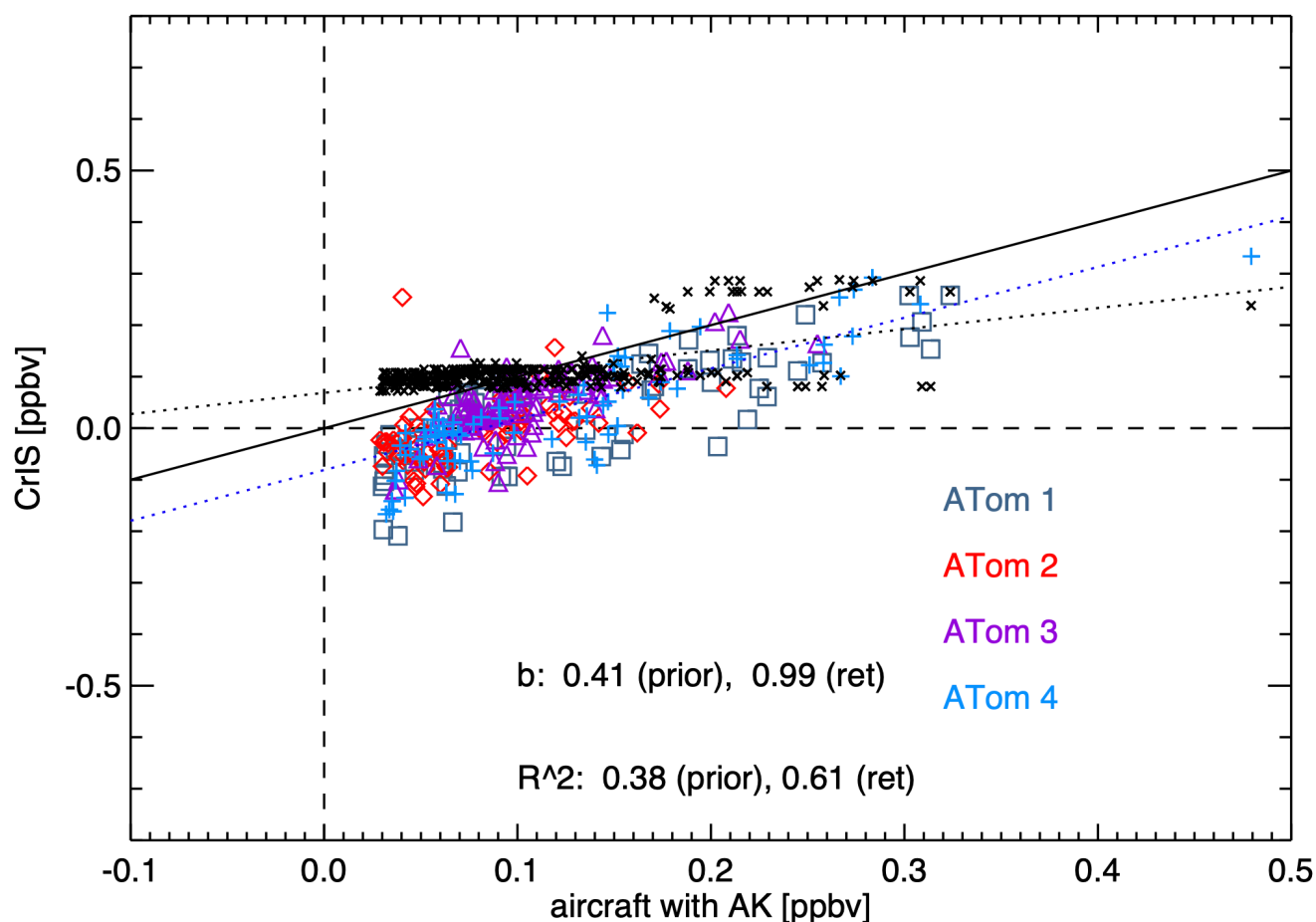
500

505

Figure 7. Scatter plot of CrIS PAN against PANTHER aircraft measurements. Colored symbols show CrIS retrieval results, while the black 'x's show the prior values used in the CrIS retrievals. CrIS results shown here are averages of the CrIS co-incidences for each of the aircraft profiles. The 1:1 line is shows as solid black, while the dashed blue and black lines show the linear fit for the CrIS retrieved and prior results respectively. Gradients (b-values) of the linear fits and R^2 values are shown on the figure.

510